LU TP 99–12
hep-ph/9906407
June 1999

Jet Production by Real and Virtual Photons[1]

C. Friberg and T. Sjöstrand

Department of Theoretical Physics, Lund University,
Helgonavägen 5, S-223 62 Lund, Sweden
christer@thep.lu.se, torbjorn@thep.lu.se

Abstract

The production of jets is studied in collisions of virtual photons, specifically for applications at HERA. Photon flux factors are convoluted with matrix elements involving either direct or resolved photons and, for the latter, with parton distributions of the photon. Special emphasis is put on the range of uncertainty in the modeling of the resolved component. The resulting model is compared with existing data and further tests are proposed.

[1] To appear in the Proceedings of the DESY Workshop on Monte Carlo Generators for HERA Physics

1 Introduction

The photon is a complicated object to describe. In the DIS region, i.e. when it is very virtual, it can be considered as devoid of any internal structure, at least to first approximation. In the other extreme, the total cross section for real photons is dominated by the resolved component of the wave function, where the photon has fluctuated into a $\mathrm{q\overline{q}}$ state. The nature of this resolved component is still not well understood, especially not the way in which it dies out with increasing photon virtuality. This dampening is likely not to be a simple function of virtuality, but to depend on the physics observable being studied, i.e. on the combination of subprocesses singled out.

Since our current understanding of QCD does not allow complete predictability, one sensible approach is to base ourselves on QCD-motivated models, where a plausible range of uncertainty can be explored. Hopefully comparisons with data may then help constrain the correct behaviour. The ultimate goal therefore clearly is to have a testable model for all aspects of the physics of $\gamma^*\mathrm{p}$ (and $\gamma^*\gamma^*$) collisions. As a stepping stone towards constructing such a framework, in this paper we explore the physics associated with the production of 'high-$p_\perp$' jets in the collision. That is, we here avoid the processes that only produce activity along the $\gamma^*\mathrm{p}$ collision axis. For resolved photons this corresponds to the 'soft' or 'low-$p_\perp$' events of the hadronic physics analogy, for direct ones to the lowest-order DIS process $\gamma^*\mathrm{q} \to \mathrm{q}$.

The processes that we will study here instead can be exemplified by $\gamma^*\mathrm{g} \to \mathrm{q\overline{q}}$ (direct) and $\mathrm{gg} \to \mathrm{q\overline{q}}$ (resolved), where the gluons come from the parton content of a resolved virtual photon or from the proton. Note that these are multi-scale processes, at least involving the virtuality Q^2 of the photon and the $p_\perp^2$ of the hard subprocess. For a resolved photon, the relative transverse momentum $k_\perp$ of the initial $\gamma^* \to \mathrm{q\overline{q}}$ branching provides a further scale, at least in our framework. This plethora of scales clearly is a challenge to any model builder, but in principle it also offers the opportunity to explore QCD in a more differential fashion than is normally possible.

At large photon virtualities, a possible strategy would be to express the cross sections entirely in terms of processes involving the photon directly, i.e. to include branchings such as $\gamma^* \to \mathrm{q'\overline{q}'}$ and $\mathrm{q'} \to \mathrm{q'g}$ in the Feynman graphs calculated to describe the process, so that e.g. the $\gamma^*\mathrm{p}$ process $\mathrm{gg} \to \mathrm{q\overline{q}}$ is calculated as $\gamma^*\mathrm{g} \to \mathrm{q'\overline{q}'q\overline{q}}$. With decreasing virtuality of the photon, such a fixed-order approach is increasingly deficient by its lack of the large logarithmic corrections generated by collinear and soft gluon emission, however. Furthermore, almost real photons allow long-lived $\gamma^* \to \mathrm{q\overline{q}}$ fluctuations, that then take on the properties of non-perturbative hadronic states, specifically of vector mesons such as the ρ^0. It is therefore that an effective description in terms of parton distributions becomes necessary. Hence the resolved component of the photon, as opposed to the direct one.

That such a subdivision is more than a technical construct is excellently illustrated by the x_γ^{obs} plots from HERA [1]. This variable sums up the fraction of the original photon lightcone momentum carried by the two highest-$E_\perp$ jets. A clear two-component structure is visible. The peak close to $x_\gamma^{\mathrm{obs}} = 1$ can be viewed as a smeared footprint of the direct photon, with all the energy partaking in the hard interaction, while the broad spectrum at lower x_γ^{obs} is consistent with the resolved photon, where much of the energy remains in a beam jet. The distinction between the two is not unique when higher-order effects are included, but it is always possible to make a functional separation that avoids double-counting or gaps.

The resolved photon can be further subdivided into low-virtuality fluctuations, which

then are of a nonperturbative character and can be represented by a set of vector mesons, and high-virtuality ones that are describable by perturbative $\gamma^* \to \mathrm{q\overline{q}}$ branchings. The former is called the VMD (vector meson dominance) component and the latter the anomalous one. The parton distributions of the VMD component are unknown from first principles, and thus have to be based on reasonable ansätze, while the anomalous ones are perturbatively predictable. This separation is more ambiguous and less well tested than the one between direct and resolved photons. In principle, studies on the structure of the beam remnant, e.g. its $p_\perp$ distribution, should show characteristic patterns. Unfortunately, the naively expected differences are smeared by higher-order QCD corrections (especially initial-state radiation), by the possibility of multiple parton–parton interactions, by hadronization effects, and so on. (Experimentally, gaps in the detector acceptance, e.g. for the beam pipe, is a further major worry.) Many of these areas offer interesting challenges in their own right; e.g. the way in which multiple interactions die out with virtuality, both that of the photon itself and that of the $\mathrm{q\overline{q}}$ pair it fluctuates to. Models for one aspect at the time are therefore likely to be inadequate. Instead we here attempt a combined description of all the relevant physics topics.

The traditional tool for handling such complex issues is the Monte Carlo approach. Our starting point is the model for real photons [2] and the parton distribution parameterizations of real and virtual photons [3] already present in the PYTHIA [4] generator. Several further additions and modifications have been made to model virtual photons, as will be described in the following. Other generators with an overlapping scope include, among others, HERWIG [5], LDC [6], LEPTO [7], PHOJET [8] and RAPGAP [9]. The details of the approaches are different, however, so this gives healthy possibilities to compare and learn. Another alternative is provided by matrix-element calculations [10], that do not provide the same complete overview but can offer superior descriptions for some purposes.

The plan of this paper is the following. In section 2 the model is described, with special emphasis on those aspects that are new compared with the corresponding description for real photons. Thereafter, in section 3, comparisons are shown with some sets of data from HERA, and this is used to constrain partly the freedom in the model. Finally, section 4 contains a summary and outlook.

2 The Model

The electromagnetic field surrounding a moving electron can be viewed as a flux of photons. Weizsäcker [11] and Williams [12] calculated the spectrum of these photons, neglecting the photon virtualities and terms involving the longitudinal polarization of photons. This approximation is well-known [13] to be a good approximation when the scattered lepton is tagged at small scattering angles.

In the equivalent photon approximation [14], the cross sections for the process $\mathrm{ep} \to \mathrm{e}\mathbf{X}$, where $\mathbf{X}$ is an arbitrary final state, can then be written as the convolution $\mathrm{d}\sigma(\mathrm{ep} \to \mathrm{e}\mathbf{X}) = \int \mathrm{d}\omega \; N(\omega) \; \mathrm{d}\sigma(\gamma\mathrm{p} \to \mathbf{X})$ where ω is the energy of the emitted photon. In this approximation, the distribution in photon frequencies $N(\omega)\mathrm{d}\omega$ is obtained by integrating over the photon virtuality Q^2. The maximum value Q^2_{max} is usually given by experimental conditions like anti-tagging, i.e. that the scattered lepton is not detected if its scattering angle is too small.

A better approximation, and the one used in our approach, is to keep the Q^2 depen-

dence in the photon flux $f(y, Q^2)$ (with $y \approx \omega/\omega_{\max}$, see below) and in the subprocess cross sections involving the virtual photon, $\gamma^* \mathrm{p} \to \mathbf{X}$, and to sum over the transverse and longitudinal photon polarizations. We then arrive with

$$\mathrm{d}\sigma(\mathrm{ep} \to \mathrm{e}\mathbf{X}) = \sum_{\xi=\mathrm{T,L}} \iint \mathrm{d}y\, \mathrm{d}Q^2\; f^{\xi}_{\gamma/\mathrm{e}}(y, Q^2)\; \mathrm{d}\sigma(\gamma^*_{\xi}\mathrm{p} \to \mathbf{X}) \; . \tag{1}$$

This factorized ansatz is perfectly general, so long as azimuthal distributions in the final state are not studied in detail.

When Q^2/W^2 is small, one can derive [16, 14, 15]

$$f^{\mathrm{T}}_{\gamma/\mathrm{e}}(y, Q^2) = \frac{\alpha_{\mathrm{em}}}{2\pi}\left(\frac{(1+(1-y)^2}{y}\frac{1}{Q^2} - \frac{2m_{\mathrm{e}}^2 y}{Q^4}\right) \; , \qquad f^{\mathrm{L}}_{\gamma/\mathrm{e}}(y, Q^2) = \frac{\alpha_{\mathrm{em}}}{2\pi}\frac{2(1-y)}{y}\frac{1}{Q^2} \; . \tag{2}$$

The y variable is defined as the lightcone fraction the photon takes of the incoming lepton momentum. In the ep kinematics, the y definition gives that

$$y = \frac{qP}{kP} \; , \qquad W^2 = ys - Q^2 \; . \tag{3}$$

(Here and in the following formulae we have omitted the lepton and hadron mass terms when it is not of importance for the argumentation.) The lepton scattering angle θ is related to Q^2, where the kinematical limits on Q^2 are, unless experimental conditions reduce the θ range, $Q^2_{\min} \approx \frac{y^2}{1-y} m_{\mathrm{e}}^2$ and $Q^2_{\max} \approx (1-y)s$.

In summary, we will allow the possibility of experimental cuts in the y, Q^2, θ and W^2 variables. Within the allowed region, the phase space is Monte Carlo sampled according to $(\mathrm{d}Q^2/Q^2)\,(\mathrm{d}y/y)\,\mathrm{d}\varphi$, with the remaining flux factor combined with the cross section factors to give the event weight used for eventual acceptance or rejection.

The hard-scattering processes are classified according to whether the photon is resolved or not. For the direct processes, QCD Compton $\gamma^*\mathrm{q} \to \mathrm{gq}$ and boson–gluon fusion $\gamma^*\mathrm{g} \to \mathrm{q}\overline{\mathrm{q}}$, both transverse and longitudinal photons are considered. The matrix elements are given elsewhere [17, 18]. Remember that the cross section for a longitudinal photon vanishes as Q^2 in the limit $Q^2 \to 0$.

For a resolved photon, there are six basic QCD cross sections, $\mathrm{qq}' \to \mathrm{qq}'$, $\mathrm{q}\overline{\mathrm{q}} \to \mathrm{q}'\overline{\mathrm{q}}'$, $\mathrm{q}\overline{\mathrm{q}} \to \mathrm{gg}$, $\mathrm{qg} \to \mathrm{qg}$, $\mathrm{gg} \to \mathrm{gg}$ and $\mathrm{gg} \to \mathrm{q}\overline{\mathrm{q}}$. The photon virtuality scale is included in the arguments of the parton distribution but, in the spirit of the parton model, the virtuality of the parton inside the photon is not included in the matrix elements. Neither is the possibility of the partons being polarized. The same subprocess cross sections as those known from pp physics [19] can therefore be used for resolved $\gamma^*\mathrm{p}$ processes. A convolution with parton distributions is then necessary.

One major element of model dependence enters via the choice of parton distributions for a resolved virtual photon. These distributions contain a hadronic component that is not perturbatively calculable. It is therefore necessary to parameterize the solution with input from experimental data, which mainly is available for (almost) real photons. In the following we will use the SaS distributions [3], which are the ones best suited for our formalism. Another set of distributions is provided by GRS [20], while a simpler recipe for suppression factors relative to real photons has been proposed by DG [21].

The SaS distributions for a real photon can be written as

$$f^{\gamma}_a(x, \mu^2) = \sum_V \frac{4\pi\alpha_{\mathrm{em}}}{f_V^2} f^{\gamma,V}_a(x, \mu^2; Q_0^2) + \frac{\alpha_{\mathrm{em}}}{2\pi} \sum_{\mathrm{q}} 2e_{\mathrm{q}}^2 \int_{Q_0^2}^{\mu^2} \frac{\mathrm{d}k^2}{k^2}\, f^{\gamma,\mathrm{q}\overline{\mathrm{q}}}_a(x, \mu^2; k^2) \; . \tag{4}$$

Here the sum is over a set of vector mesons $V = \rho^0, \omega, \phi, \mathrm{J}/\psi$ according to a vector-meson-dominance ansatz for low-virtuality fluctuations of the photon, with experimentally determined couplings $4\pi\alpha_{\mathrm{em}}/f_V^2$. The higher-virtuality, perturbative, fluctuations are represented by an integral over the virtuality k^2 and a sum over quark species. We will refer to the first part as the VMD one and the second as the anomalous one.

From the above ansatz, the extension to a virtual photon is given by the introduction of a dipole dampening factor for each component,

$$\begin{aligned} f_a^{\gamma^*}(x,\mu^2,Q^2) &= \sum_V \frac{4\pi\alpha_{\mathrm{em}}}{f_V^2}\left(\frac{m_V^2}{m_V^2+Q^2}\right)^2 f_a^{\gamma,V}(x,\mu^2;\tilde{Q}_0^2) \\ &+ \frac{\alpha_{\mathrm{em}}}{2\pi}\sum_{\mathrm{q}} 2e_{\mathrm{q}}^2 \int_{Q_0^2}^{\mu^2}\frac{\mathrm{d}k^2}{k^2}\left(\frac{k^2}{k^2+Q^2}\right)^2 f_a^{\gamma,\mathrm{q}\overline{\mathrm{q}}}(x,\mu^2;k^2)\ . \end{aligned} \tag{5}$$

Thus, with increasing Q^2, the VMD components die away faster than the anomalous ones, and within the latter the low-k^2 ones faster than the high-k^2 ones. As a technical trick, the handling of the k^2 integral is made more tractable by replacing the dipole factor by a k^2-independent multiplicative factor and an increased lower limit of the integral, in such a way that both the momentum sum and the average evolution range is unchanged. Finally, correction factors are introduced to ensure that $f_a^{\gamma^*}(x,\mu^2,Q^2) \to 0$ for $\mu^2 \to Q^2$: in the region $Q^2 > \mu^2$ a fixed-order perturbative description is more appropriate than the leading-log description in terms of a resolved photon.

Since the probed real photon is purely transverse, the above ansatz does not address the issue of parton distributions of the longitudinal virtual photons. One could imagine an ansatz based on longitudinally polarized vector mesons, and branchings $\gamma_{\mathrm{L}}^* \to \mathrm{q}\overline{\mathrm{q}}$, but currently no parameterization exists along these lines. We will therefore content ourselves by exploring a simple alternative based on applying a simple multiplicative factor R to the results obtained for a resolved transverse photon. As usual, processes involving longitudinal photons should vanish in the limit $Q^2 \to 0$. To study two extremes, the region with a linear rise in Q^2 is defined either by $Q^2 < \mu^2$ or by $Q^2 < m_\rho^2$, where the former represents the perturbative and the latter some non–perturbative scale. Also the high-Q^2 limit is not well constrained; we will compare two different alternatives, one with an asymptotic fall-off like $1/Q^2$ and another which approaches a constant ratio, both with respect to the transverse resolved photon. (Since we put $f_a^{\gamma^*}(x,\mu^2,Q^2) = 0$ for $Q^2 > \mu^2$, the R value will actually not be used for large Q^2, so the choice is not so crucial.) We therefore study the alternative ansätze

$$R_1(y,Q^2,\mu^2) = 1 + a\frac{4\mu^2Q^2}{(\mu^2+Q^2)^2}\frac{f_{\gamma/l}^{\mathrm{L}}(y,Q^2)}{f_{\gamma/l}^{\mathrm{T}}(y,Q^2)}\ , \tag{6}$$

$$R_2(y,Q^2,\mu^2) = 1 + a\frac{4Q^2}{(\mu^2+Q^2)}\frac{f_{\gamma/l}^{\mathrm{L}}(y,Q^2)}{f_{\gamma/l}^{\mathrm{T}}(y,Q^2)}\ , \tag{7}$$

$$R_3(y,Q^2,\mu^2) = 1 + a\frac{4Q^2}{(m_\rho^2+Q^2)}\frac{f_{\gamma/l}^{\mathrm{L}}(y,Q^2)}{f_{\gamma/l}^{\mathrm{T}}(y,Q^2)} \tag{8}$$

with $a = 1$ as main contrast to the default $a = 0$. The y dependence compensates for the difference in photon flux between transverse and longitudinal photons.

Another ambiguity is the choice of μ^2 scale in parton distributions. Based on various

considerations, we compare six different alternatives:

$$\mu_1^2 = p_\perp^2 \,, \tag{9}$$

$$\mu_2^2 = p_\perp^2 \, \frac{\hat{s} + xQ^2}{\hat{s}} \,, \tag{10}$$

$$\mu_3^2 = p_\perp^2 \, \frac{\hat{s} + Q^2}{\hat{s}} \,, \tag{11}$$

$$\mu_4^2 = p_\perp^2 + \frac{Q^2}{2} \,, \tag{12}$$

$$\mu_5^2 = p_\perp^2 + Q^2 \,, \tag{13}$$

$$\mu_6^2 = 2\mu_3^2 \,. \tag{14}$$

Only the fifth alternative ensures $f_a^{\gamma^*}(x, \mu^2, Q^2) > 0$ for arbitrarily large Q^2; in all other alternatives the resolved contribution (at fixed $p_\perp$) vanish above some Q^2 scale. The last alternative exploits the well-known freedom of including some multiplicative factor in any (leading-order) scale choice. When nothing is mentioned explicitly below, the choice μ_3^2 is used.

The issues discussed above are the main ones that distinguish the description of processes involving virtual photons from those induced by real photons or by hadrons in general. In common is the need to consider the buildup of more complicated partonic configurations from the lowest-order 'skeletons' defined above, (*i*) by parton showers, (*ii*) by multiple parton–parton interactions and beam remnants, where applicable, and (*iii*) by the subsequent transformation of these partons into the observable hadrons. The latter, hadronization stage can be described by the standard string fragmentation framework [22], followed by the decays of unstable primary hadrons, and is not further discussed here. The parton shower, multiple-interaction and beam-remnant aspects are discussed elsewhere [18].

3 Comparisons with Data

In this section the model is compared with data. We will not make a detailed analysis of experimental results but use it to point out model dependences and to constrain some model parameters.

$2 \to 2$ parton interactions normally give rise to 2–jet events. In leading–order QCD, the jets are balanced in transverse momenta in the centre of mass frame of the γ^*p subsystem. Various effects, such as primordial $k_\perp$, initial- and final-state bremsstrahlung, tend to spoil this picture. This increases the $\mathrm{d}\sigma/\mathrm{d}p_\perp$ spectrum at any fixed $p_\perp$, since jets can be boosted up from lower $p_\perp$. In order to study jets above some $p_{\perp,\mathrm{min}}^{\mathrm{jet}}$, typically a $p_{\perp,\mathrm{min}}^{\mathrm{parton}} = \frac{1}{2} p_{\perp,\mathrm{min}}^{\mathrm{jet}}$ or less is required in the generation procedure.

3.1 Inclusive ep Jet Cross Sections

Inclusive ep jet cross sections have been measured by the H1 collaboration [23] in the kinematical range $0 < Q^2 < 49$ GeV^2 and $0.3 < y < 0.6$. The differential jet cross sections $\mathrm{d}\sigma_{\mathrm{ep}}/\mathrm{d}E_\perp^*$ and $\mathrm{d}\sigma_{\mathrm{ep}}/\mathrm{d}\eta^*$ in Fig. 1 and 2 respectively, were produced with the HzTool [24] package. The $E_\perp^*$ and η^* are calculated in the γ^*p centre of mass frame where the incident proton direction corresponds to positive η^*.

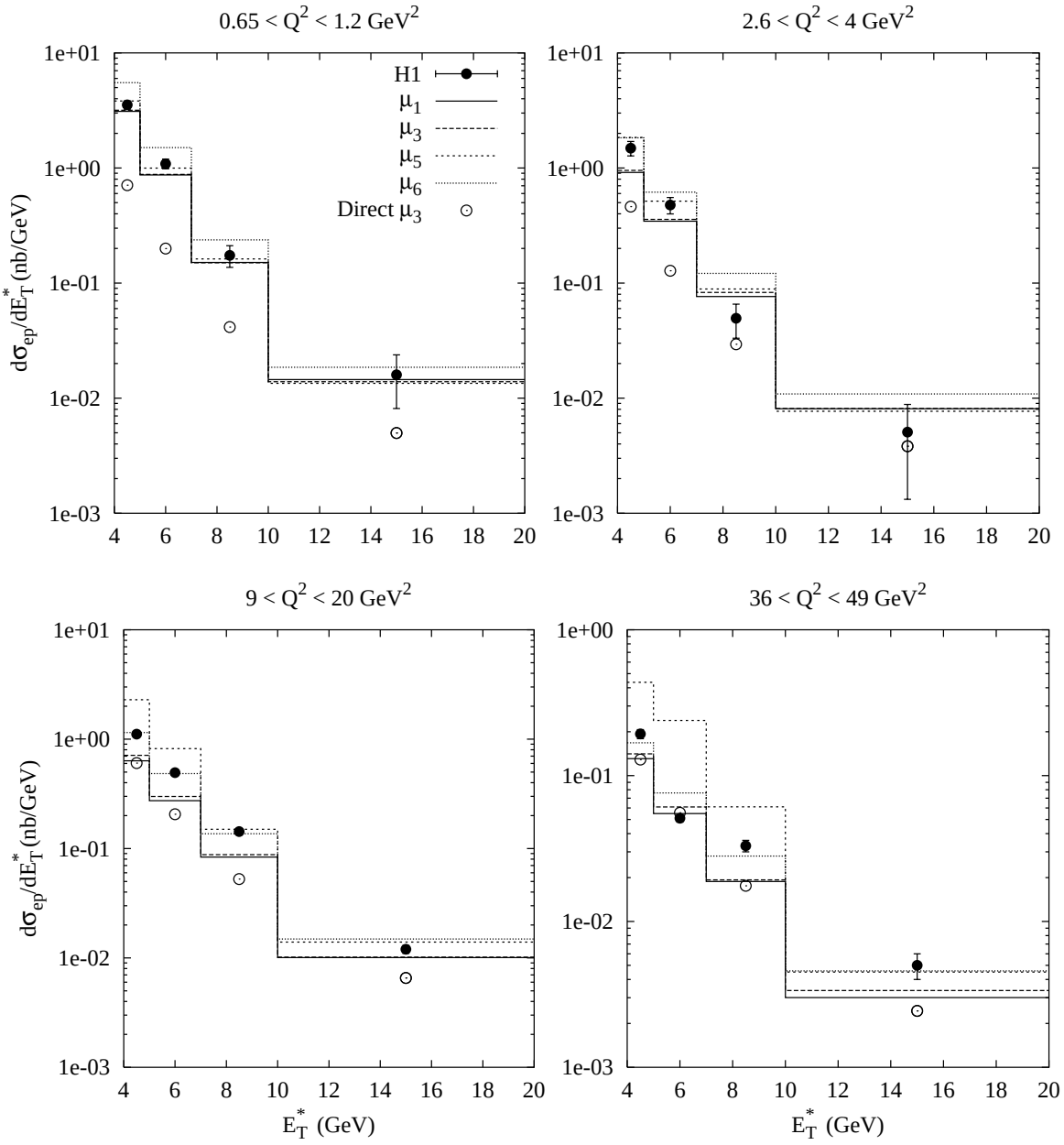

Figure 1: *The differential jet cross section* $\mathrm{d}\sigma_{\mathrm{ep}}/\mathrm{d}E_\perp^*$ *for jets with* $-2.5 < \eta^* < -0.5$ *and* $0.3 < y < 0.6$.

For $\mathrm{d}\sigma_{\mathrm{ep}}/\mathrm{d}E_\perp^*$ and $\mathrm{d}\sigma_{\mathrm{ep}}/\mathrm{d}\eta^*$ data is available in nine different Q^2 bins; some of them are shown here with similar results for the intermediate bins. The SaS 1D parton distribution together with a few different μ_i scales are used to model the resolved photon component. The other choices of scales, μ_2^2 and μ_4^2, interpolates between these results.

In the highest Q^2 bin the direct component is the dominant contribution; the virtuality of the photon is for most events of the order of or larger than the transverse momenta squared, $Q^2 \gtrsim p_\perp^2$. However, the resolved component is not negligible and all the scales μ_i, except μ_1, depend on the photon virtuality. This gives a larger resolved component in this region as compared to the the conventional choice, $\mu_1 = p_\perp$. In the low Q^2 bin the μ_i scales do not differ much from $p_\perp$, i.e. the results are not sensitive to the scale choice

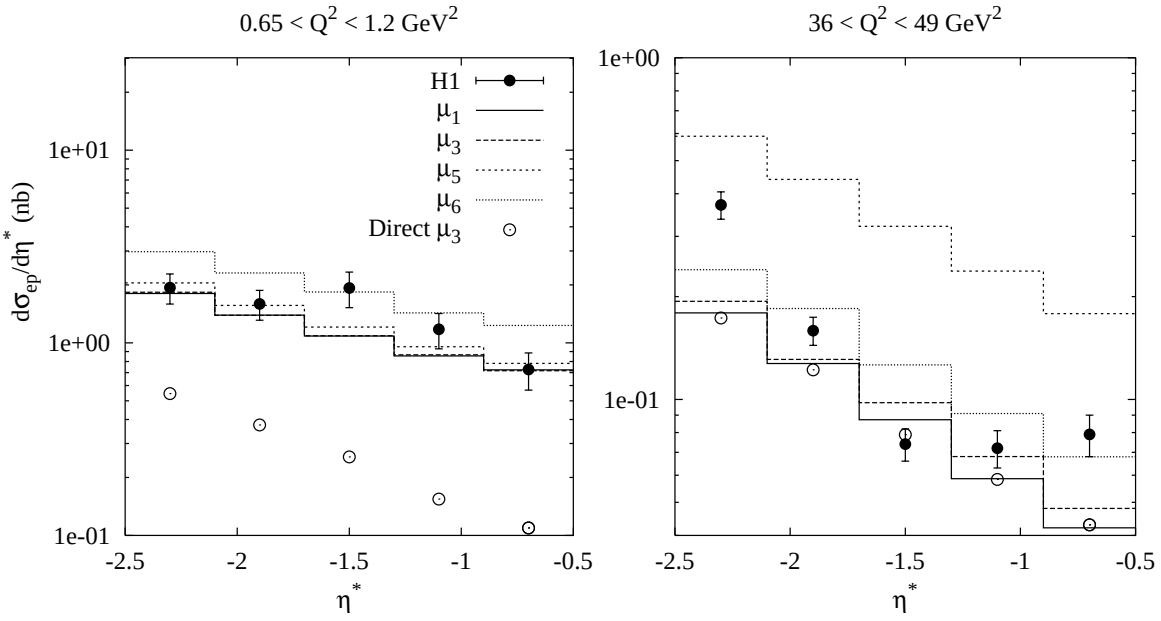

Figure 2: *The differential jet cross section* $\mathrm{d}\sigma_{\mathrm{ep}}/\mathrm{d}\eta^*$ *for jets with* $E_\perp^* > 5$ GeV *and* $0.3 < y < 0.6$.

μ_i. The exception is μ_6, which there overshoots the data. The $\mu_4 = p_\perp^2 + Q^2/2$ scale (not shown) gives nice agreement with data for all different Q^2 bins.

Changing the photon parton distribution from SaS 1D to SaS 2D will give a slightly lower result for the low Q^2 bins (for most points within the size of the symbols). Using CTEQ 3L instead of GRV leading order as the proton parton distribution reduce the result in some $E_\perp^*$ and η^* bins by half. The GRV higher order parton distribution give a slightly lower result (as compared to GRV leading order).

Since the VMD part dies out quickly with increasing photon virtuality, multiple interactions will only be visible at low Q^2 (multiple interactions for the anomalous component is not in the model so far). The anomalous component dominates over the VMD component already at 1 GeV^2. Therefore, multiple interactions for the VMD component can safely be neglected for the distributions shown in this section.

3.2 Forward Jets in ep

Jet cross sections as a function of Bjorken-x, x_{Bj}, for forward jet production (in the proton direction) have been measured at HERA [25]. The objective is to probe the dynamics of the QCD cascade at small x_{Bj}. The forward jet is restricted in polar angle w.r.t. the proton and the transverse momenta $p_\perp^{\mathrm{jet}}$ should be of the same order as the virtuality of the photon, suppressing an evolution in transverse momenta. If the jet has a large energy fraction of the proton there will be a big difference in x between the jet and the photon vertex; $x_{\mathrm{Bj}} \ll x_{\mathrm{jet}}$, allowing an evolution in x. The above restrictions will not eliminate the possibility of having a resolved photon, although the large Q^2 values are not in favour of it.

The HzTool routines [24] were used to obtain the results in Fig. 3. Four different scales μ_i are shown. A larger forward jet cross section is obtained with a stronger Q^2

dependence, with the scale $\mu_5^2 = p_\perp^2 + Q^2$ in best agreement with data [26]. The choice of scale does not only affect the resolved photon contribution but also the direct photon, arising from the scale dependence in the proton parton distribution, as seen in Fig. 4. The rather large Q^2 values, $Q^2 \simeq (p_\perp^{\rm jet})^2$, suppresses VMD photons and favours the SaS 1D distribution which is the one used here, though the difference is small.

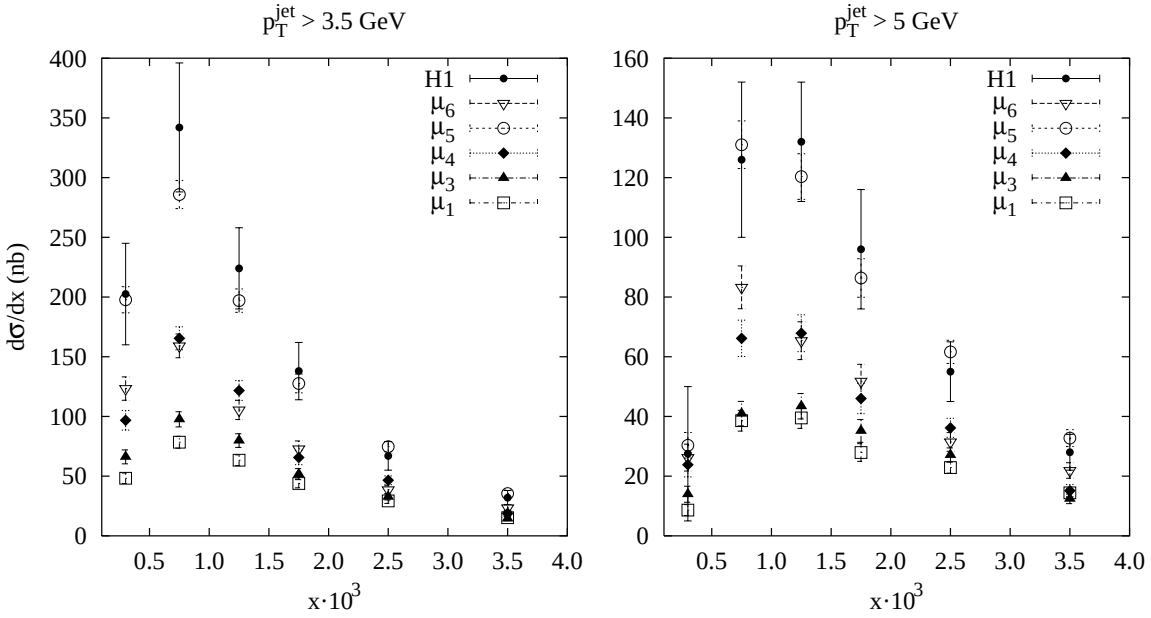

Figure 3: *Forward jet cross section as a function of x compared with H1 data (with statistical and systematic uncertainties added in quadrature). Five different scales are shown at two different $p_\perp^{\rm jet}$ cuts,* 3.5 *and* 5 GeV. $x_{\rm jet} > 0.035$, $0.5 < (p_\perp^{\rm jet})^2/Q^2 < 2$ *and* $7^\circ < \theta_{\rm jet} < 20^\circ$.

Note that the μ_6 scale undershoots the forward jet cross section data and overshoots the inclusive jet distributions at low Q^2, so it is not a real alternative. As a further check, with more data accumulated and analysed, the $(p_\perp^{\rm jet})^2/Q^2$ interval could be split into several subranges which hopefully would help to discriminate between scale choices.

3.3 Importance of longitudinal resolved photons

In this section we will study the importance of longitudinal resolved photons. A sensible Q^2–dependent scale choice, μ_3, together with the SaS 1D distribution will be used throughout.

With $a = 1$ the different alternatives are shown in Fig. 5 for the $\mathrm{d}\sigma_{\rm ep}/\mathrm{d}E_\perp^*$ distributions together with the result from pure transverse photons, i.e. $a = 0$. The importance of the resolved contributions decreases with increasing Q^2, see Fig. 1, which makes the asymptotic behaviour less crucial. The onset of longitudinal photons governed by the R_1 and R_2 alternatives are favoured whereas the R_3 one overshoots data in the context of the other model choices made here.

In Fig. 6 the same alternatives are shown for the forward jet cross sections. With this scale choice, μ_3, none of the longitudinal resolved components (together with the direct contribution) are sufficient to describe the forward jet cross section. The resolved

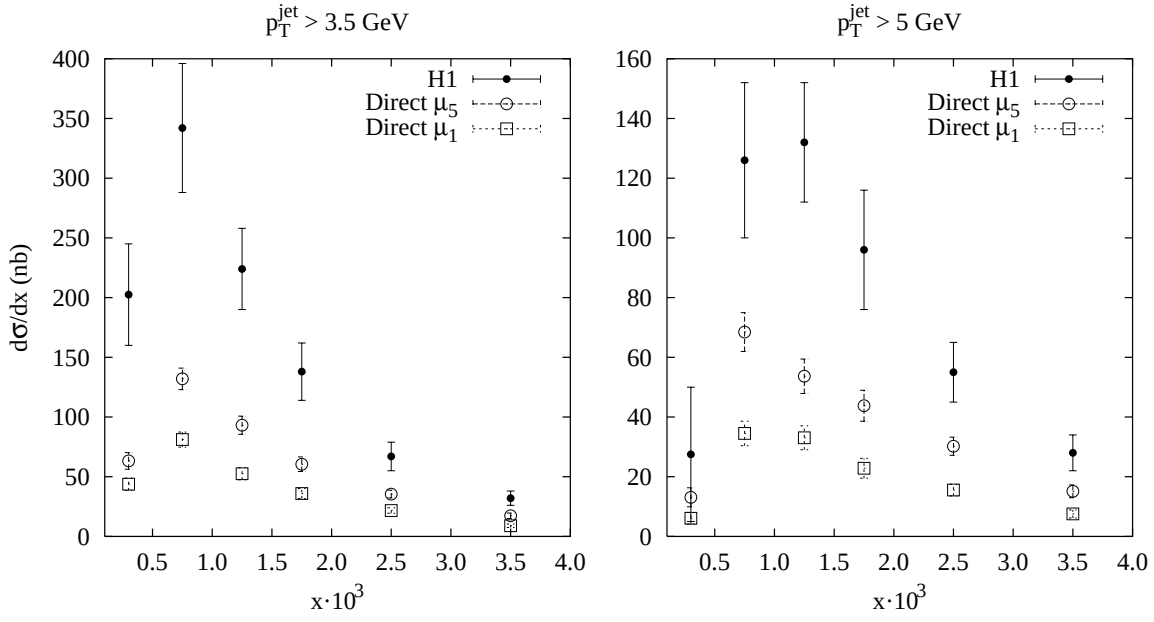

Figure 4: *Same as in Fig. 3 but only the direct component is compared with data for two different scale choices.*

contribution with R_3 is about the same as the one obtained with the scale $\mu_5^2 = p_\perp^2 + Q^2$ (without longitudinal contribution); the difference in the total results originates from the difference in the direct contributions, see Fig. 4. With R_1 and $a = 1$, the μ_5 scale (not shown) overshoots the data, but undershoots in combination with μ_4.

The above study indicates, as expected, that longitudinal resolved photons are important for detailed descriptions of various distributions. It cannot by itself explain the forward jet cross section, but may give a significant contribution. Combined with other effects, for example, different scale choice, parton distributions and underlying events, it could give a reasonable description. The model(s) so far does not take into account the difference in x distribution or the k^2 scale (of the $\gamma^* \to \mathrm{q\overline{q}}$ fluctuations) between transverse and longitudinal photons. As long as the distributions under study allow a large interval in x the average description may be reasonable. In a more sophisticated treatment these aspects have to be considered in more detail.

4 Summary and Outlook

The field of photon physics is rapidly expanding, not least by the impact of new data from HERA and LEP. The prospects of building a Linear Collider, with its objective of high-precision measurements and to search for possible new physics, requires an accurate description of photon processes. The plan here is to have a complete description of the main physics aspects in γp and $\gamma\gamma$ collisions, which will allow important cross checks to test universality of certain model assumptions. As a step forward, we have in this study concentrated on those that are of importance for the production of jets by virtual photons, and are absent in the real-photon case. While we believe in the basic machinery developed and presented here, we have to acknowledge the many unknowns — scale choice, parton distribution sets, longitudinal contributions, underlying events, etc. — that all give non–

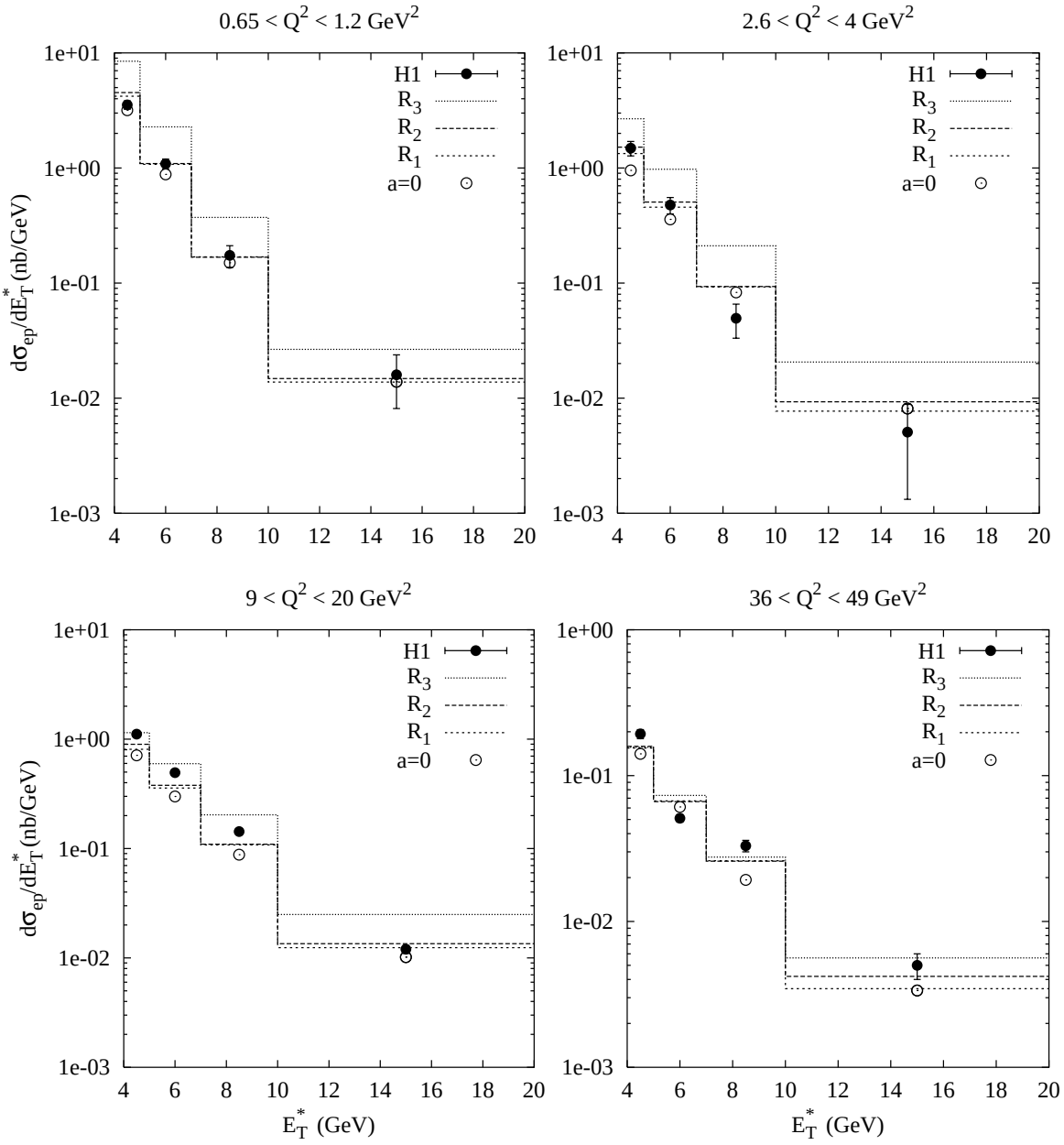

Figure 5: *The differential jet cross section* $\mathrm{d}\sigma_{\mathrm{ep}}/\mathrm{d}E^*_\perp$ *for jets with* $-2.5 < \eta^* < -0.5$ *and* $0.3 < y < 0.6$.

negligible effects. To make a detailed tuning of all these aspects was not the aim here, but rather to point out model dependences that arise from a virtual photon.

When Q^2 is not small, naively only the direct component needs to be treated, but in practice a rather large contribution arises from resolved photons. For example, for high Q^2 studies like forward jet cross sections, Fig. 3 and 4, or inclusive differential jet cross sections, Fig. 1 and 2. Resolved longitudinal photons are poorly understood and the model(s) presented here can be used to estimate their importance and get a reasonable global description. Longitudinal effects are in most cases small but of importance for fine–tuning.

The forward jet cross section presented by H1 [25] is well described by an ordinary

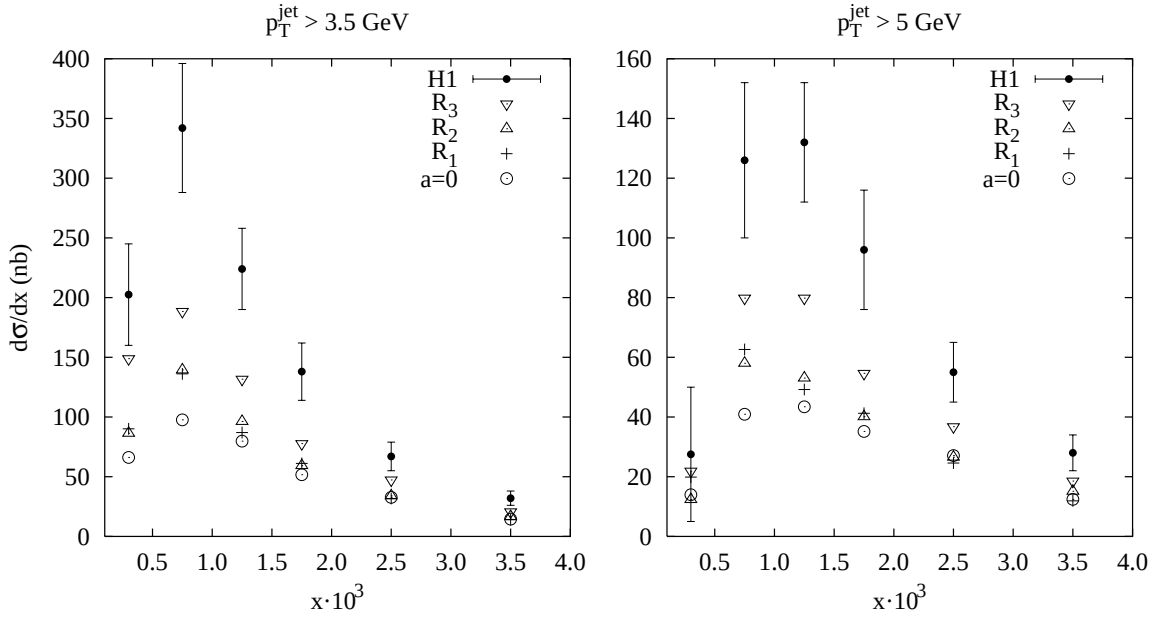

Figure 6: *Forward jet cross section as a function of x. The results with three different alternatives of longitudinal resolved photons R_i are compared with purely transverse ones, $a = 0$, and data from H1.*

parton shower prescription including the possibility of having resolved photons. The criteria that the $p_\perp^{\rm jet}$ should be of the same order as Q^2, makes the scale choice crucial and in favour of data is $\mu_5^2 = p_\perp^2 + Q^2$. With more data accumulated and analysed, the $(p_\perp^{\rm jet})^2/Q^2$ interval could be split into several subranges, which hopefully would help to discriminate between different scale choices.

After this study of jet production by virtual photons it is natural to connect it together with low–$p_\perp$ events. Clearly, a smooth transition from perturbative to non–perturbative physics is required. Further studies are needed and will be presented in a future publication.

Acknowledgements

We acknowledge helpful conversations with, among others, Jon Butterworth, Jiri Chýla, Gerhard Schuler, Hannes Jung, Leif Jönsson, Ralph Engel and Tancredi Carli.

References

[1] ZEUS Collaboration, M. Derrick et al., *Phys. Lett.* **B322**, 287 (1994);
H1 Collaboration, T. Ahmed et al., *Nucl. Phys.* **B445**, 195 (1995).

[2] G.A. Schuler and T. Sjöstrand, *Nucl. Phys.* **B407**, 539 (1993): *Z. Phys.* **C73**, 677 (1997).

[3] G.A. Schuler and T. Sjöstrand, *Z. Phys.* **C68**, 607 (1995); *Phys. Lett.* **B376**, 193 (1996).

[4] T. Sjöstrand, *Computer Phys. Commun.* **82**, 74 (1994);
http://www.thep.lu.se/~torbjorn/Pythia.html.

[5] G. Marchesini, B.R. Webber, G. Abbiendi, I.G. Knowles, M.H. Seymour and L. Stanco, *Computer Phys. Commun.* **67**, 465 (1992).

[6] H. Kharraziha and L. Lönnblad, *J. High Energy Phys.* **03**, 006 (1998).

[7] G. Ingelman, A. Edin and J. Rathsman, *Computer Phys. Commun.* **101**, 108 (1997).

[8] R. Engel and J. Ranft, *Phys. Rev.* **D54**, 4244 (1996).

[9] H. Jung, *Computer Phys. Commun.* **86**, 147 (1995).

[10] M. Glück, E. Reya and M. Stratmann, *Phys. Rev.* **D54**, 5515 (1996);
D. de Florian, C. Garcia Canal and R. Sassot, *Z. Phys.* **C75**, 265 (1997);
M. Klasen, G. Kramer and B. Pötter, *Eur. Phys. J.* **C1**, 261 (1998).

[11] C.F. von Weiszäcker, *Z. Phys.* **88**, 612 (1934).

[12] E.J. Williams, *Phys. Rev.* **45**, 729 (1934).

[13] M. Klasen, G. Kramer and S.G. Salesch, *Z. Phys.* **C68**, 113 (1995)

[14] V.M. Budnev, I.F. Ginzburg, G.V. Meledin and V.G. Serbo,
Phys. Rep. **15**, 181 (1975).

[15] G.A. Schuler, *Computer Phys. Commun.* **108**, 279 (1998).

[16] G. Bonneau, M. Gourdin and F. Martin, *Nucl. Phys.* **B54**, 573 (1973).

[17] G. Altarelli and G. Martinelli, *Phys. Lett.* **B76**, 89 (1978);
A. Mendéz, *Nucl. Phys.* **B145**, 199 (1978);
R. Peccei and R. Rückl, *Nucl. Phys.* **B162**, 125 (1980);
Ch. Rumpf, G. Kramer and J. Willrodt, *Z. Phys.* **C7**, 337 (1981).

[18] C. Friberg and T. Sjöstrand, LU TP 99–11

[19] B.L. Combridge, J. Kripfganz and J. Ranft, *Phys. Lett.* **B70**, 234 (1977);
R. Cutler and D. Sivers, *Phys. Rev.* **D17**, 196 (1978).

[20] M. Glück, E. Reya and M. Stratmann, *Phys. Rev.* **D51**, 3220 (1995).

[21] F.M. Borzumati and G.A. Schuler, *Z. Phys.* **C58**, 139 (1993);
M. Drees and R.M. Godbole, *Phys. Rev.* **D50**, 3124 (1994).

[22] B. Andersson, G. Gustafson, G. Ingelman and T. Sjöstrand,
Phys. Rep. **97**, 31 (1983).

[23] H1 Collaboration, C. Adloff et al., *Phys. Lett.* **B415**, 418 (1997).

[24] J. Bromley et al.,
HzTool — A Package for Monte Carlo Generator – Data Comparison at HERA,
http://dice2.desy.de/~h01rtc/hztool.html.

[25] H1 Collaboration, C. Adloff et al., *Nucl. Phys.* **B538**, 3 (1998);
H1 Collaboration, S. Aid et al., *Phys. Lett.* **B356**, 118 (1995);
ZEUS Collaboration, J. Breitweg et al., *Eur. Phys. J.* **C6**, 239 (1998).

[26] H. Jung, L. Jönsson and H. Kuster, DESY-98-051 (hep-ph/9805396).